# Enhanced cryogenic and ambient temperature mechanical properties of CoCuFeMnNi high entropy alloy through controlled heat treatment

J. Fiocchi[1,2,*], A. Mostaed[3], M. Coduri[4], A. Tuissi[1], R. Casati[2,*]

[*] corresponding authors: jacopo.fiocchi@icmate.cnr.it ; riccardo.casati@polimi.it

1 CNR ICMATE, unit of Lecco, via Previati 1/e, 23900, Lecco, Italy

2 Politecnico di Milano, Department of Mechanical Engineering, via la G. La Masa 1, 20156, Milano, Italy

3 University of Oxford, Department of Materials, Parks Road, Oxford OX1 3PH, UK

4 University of Pavia, Department of Chemistry, viale Taramelli 16, 27100, Pavia, Italy.

**Abstract**

Dedicated thermal treatments can improve the mechanical behaviour of high entropy alloys (HEAs) by producing nanostructured microstructures with improved characteristics. Herein, the inherent metastability of an equiatomic CoCuFeMnNi alloy was exploited to induce the formation of secondary phases upon ageing treatment. Advanced characterization techniques, namely high resolution synchrotron X-ray diffraction and aberration corrected scanning transmission electron microscopy, allowed to describe the decomposition of the supersaturated solid solution. Nanometric rounded Cu-rich clusters in the solution-treated alloy and coherent, regularly oriented Cu-rich discs in the peak-aged condition were possibly produced by spinodal decomposition. An almost 100 % enhancement of mechanical strength was obtained thanks to the modulation of composition. Moreover, mechanical behaviour at cryogenic temperature was improved by ageing, both in terms of strength and ductility. Plastic deformation took place by dislocation slip, regardless of the testing temperature.

**Keywords**

High entropy alloy; spinodal decomposition; CoCuFeMnNi; high resolution synchrotron X-ray diffraction; aberration corrected scanning transmission electron microscopy.

## 1. Introduction

Since their introduction in 2004, high entropy alloys (HEAs) [1] have attracted considerable research interest and have paved the way to the design and development of an astonishing variety of new formulations. Nowadays, the pursuit for materials with improved mechanical properties has become a strong drive for the development of specifically designed HEAs, or multi-phase compositionally complex alloys, that are strengthened through different mechanisms, including grain refinement [2,3], twinning [4], transformation induced plasticity [5,6], and precipitation hardening [7]. The most studied HEAs are based on transition metals, as the CoCrFeMnNi (Cantor alloy), that was the object of many recent investigations [8]. In 2016, a variant of the Cantor alloy, which is based on the substitution of Cr with Cu, was proposed by Tazuddin and co-workers [9,10]. The CoCuFeMnNi showed the possibility of obtaining a single face centred cubic (FCC) phase after homogenization treatment followed by water quenching [11]. A number of works highlighted the unstable nature of the FCC phase in CoCuFeMnNi structure that promotes the formation of second phases at high temperatures [11–13]. In particular, Sonkusare et al. [12] studied the decomposition of the FCC phase at temperatures between 450 °C and 650 °C, and they concluded that Cu atoms diffuse to grain boundaries leading to the formation of a Cu-rich FCC phase [11]. Mac Donald and co-workers [13] studied the effect of post-deformation annealing treatments and they concluded that annealing at temperatures below 600 °C causes the precipitation of an ordered body centred cubic (BCC) phase rich in Fe and Co, whereas a Cu-rich FCC second phase was obtained in the 600 °C – 900 °C interval. These phases were found able to improve mechanical properties of the alloy. A peculiar microstructure emerged in the homogenized CoCuFeMnNi alloy subjected to 0.2 % deformation, where the initial FCC phase separated into two intercalated phases, with different content of Cu but same lattice parameter [14].

Thus far, the available knowledge on CoCuFeMnNi shows the possibility of tailoring its microstructure and mechanical performance through controlled heat treatments. To the best of Authors' knowledge, no published paper focused on controlled decomposition of supersaturated solid solution through ageing treatment of the CoCuFeMnNi alloy. Such treatment is commonly applied to a variety of alloys, including aluminium alloys [15], steels [16] and nickel-based alloys [17], and allows fine-tuning the nature, size and morphology of precipitates, thus leading to improved mechanical properties. In fact, similar heat treatments have been applied to other families of specifically designed high entropy alloys, too, resulting in an impressive improvement of mechanical properties [18,19]. In this view, the present work aims at enhancing mechanical properties of the CoCuFeMnNi HEA through a properly designed heat treatment schedule. The heat treatment parameters were designed based on results of CALPHAD simulations of phase stability and by monitoring the evolution of material hardness as a function of time and temperature. The microstructure of the alloy in different heat treatment conditions was investigated at multiple length-scales by advanced characterization techniques, including high resolution synchrotron X-ray diffraction (S-XRD) and aberration corrected scanning transmission electron microscopy (ac-STEM). Finally, the correlation between the alloy microstructure and its tensile behaviour was investigated at room and cryogenic

temperature. In fact, HEAs have been proposed for numerous applications which involve prolonged exposition to extremely low temperatures, such as offshore plants, transportation of liquid fuels and energy industry [20]. Such interest is driven by the optimal combination of increased strength and improved ductility, which HEAs frequently show at cryogenic temperatures thanks to the activation of specific plastic deformation mechanisms [21].

## 2. Materials and experimental procedures

Buttons of equiatomic CoCuFeMnNi alloy were produced by vacuum arc remelting (VAR) of pure raw materials under low pressure Ar atmosphere. They were remelted 6 times inside a water-cooled copper crucible to ensure high compositional homogeneity. The ingots were pressed at room temperature and cold rolled down to 1 mm-thick strips (80 % cold work).

Thermocalc (TCHEA4 database) software was used to calculate phase stability diagram and to select temperatures for heat treatments. The strips were solution-treated under flowing Ar atmosphere at 1000 °C for 1 h, quenched in water at ambient temperature (25 °C) and then aged at three temperatures between 530 °C and 630 °C for different times (Figure 1 a).

Microstructural characterization of solution-treated and peak-aged samples was performed through different techniques. The crystalline structure of the alloy was investigated by X-ray diffraction (XRD), employing a laboratory XRD system (Panalytical X'PertPro, wavelength = 1.5418 Å) for preliminary analysis and a synchrotron-based one (S-XRD) for high-resolution observations. High resolution Synchrotron Diffraction data were collected at 25°C at the ID22 beamline of the ESRF, in Grenoble, in transmission geometry at incident wavelength $\lambda$ = 0.3545 Å (about 35 keV). The high resolution is provided by Si (111) crystal analysers intercepting the diffracted beam. The signal is recorded with a 2D Eiger detector, positioned behind the crystal analysers [22]. The wavelength was calibrated with Si Nist 640 powder reference. The specimens were shaped on purpose in the form of finely polished small bars, about 20 mm long and 1 mm thick in order to fit the sample holder. Reducing the thickness is crucial to minimize sample absorption, yet guaranteeing random grain orientation. To this purpose, the specimens were rotated during acquisition. The diffraction signal was recorded to get full statistics in the 2θ range between 3° and 50°, corresponding to about 0.9 - 15 $Å^{-1}$ momentum transfer Q.

Metallographic analysis of selected conditions was performed by field emission scanning electron microscope (FE-SEM, Zeiss Gemini) on finely polished and etched (Nital 2% reagent) samples. Samples were prepared for STEM analysis using standard routes, i.e. first, grinding and polishing the specimens to < 50 μm and then ion beam milling to electron transparency. Ion beam milling was performed at room

temperature by a Fischione Ion Mill 1010 using $Ar^+$ initially at 6 keV and final milling at 1 keV. Finally, a JEOL ARM-200F operated at 200 keV, equipped with energy-dispersive x-ray (EDX) spectrometer was used to investigate the structure of the specimens down to atomic scale.

Mechanical properties were evaluated through micro-hardness (Future-Tech FM-810, applying a 300 gf load for 15 s) and tensile tests at room temperature and -70 °C (MTS 2/M, strain rate 0.015 $min^{-1}$). Used sub-size specimens were designed according to E8/E8M-11 ASTM standard. They showed an overall length of 100 mm and a thickness of 1 mm; the reduced section was 32 mm long and 4 mm large; the grip sections measured 10 mm x 30 mm. Post-mortem metallographic analyses were conducted by optical microscopy (Leitz Aristomet) on broken tensile specimens to investigate plastic deformation mechanisms.

## 3. Results and discussion

The diagram of Figure 1 b shows the evolution of equilibrium phases as a function of temperature. Based on numerical results, solution treatment temperature (i.e. 1000°C) was selected within the FCC single-phase field (FCC1), whereas ageing temperatures, namely 530°C, 580 °C and 630 °C are expected to produce further thermodynamically stable phases. At 580 °C and 630 °C, a second FCC phase (FCC2) is predicted to form from the parent FCC1 phase, whereas at 530°C a BCC phase is expected along with the two FCC phases. The hardness trends of the solution-treated alloy as a function of ageing time are illustrated in Figure 1 c. The CoCuFeMnNi alloy shows a similar behaviour during ageing at 630 °C and 580 °C, both in terms of achievable hardening magnitude and dependency on treatment duration. Their trends are characterized by a steep hardness increase in the initial stage of the treatment, from 141 HV of the solution-treated condition to 229 HV after 45 min at 630 °C. Thereafter, a shallower increase up to the maximum hardness value (246 HV after 6 h at 630 °C) occurs. Finally, a limited overageing effect is noticeable for longer durations. At 530 °C, some evidence of a two-step hardening process is visible, with a hardness plateau dividing the initial steep increase from the following shallower hardness gain. Such different behaviour could be related to the formation of different phases during the treatment at 530°C, i.e. the BCC and FCC2 phases predicted by CALPHAD simulation and that also detected by XRD analysis, as shown by the diffractogram of Figure 1 d. This is also in good agreement with the findings of MacDonald et al. in ref. [13], where a Fe- and Co-rich BCC phase was found in rolled CoCuFeMnNi alloy that was annealed at 600 °C. On the contrary, reflections related to FCC phases only were detected in samples aged at 580 °C and 630 °C, which also agrees with CALPHAD predictions.

Further microstructural investigations and mechanical testing results, which will be described in the following paragraphs, were performed on samples displaying the lowest and highest hardness, i.e. the solution-treated samples and those aged at 630 °C for 6 h, respectively. For the sake of brevity, the peak-

aged nomenclature will be used for samples which underwent solution treatment at 1000 °C, followed by water quenching and ageing at 630 °C for 6 h.

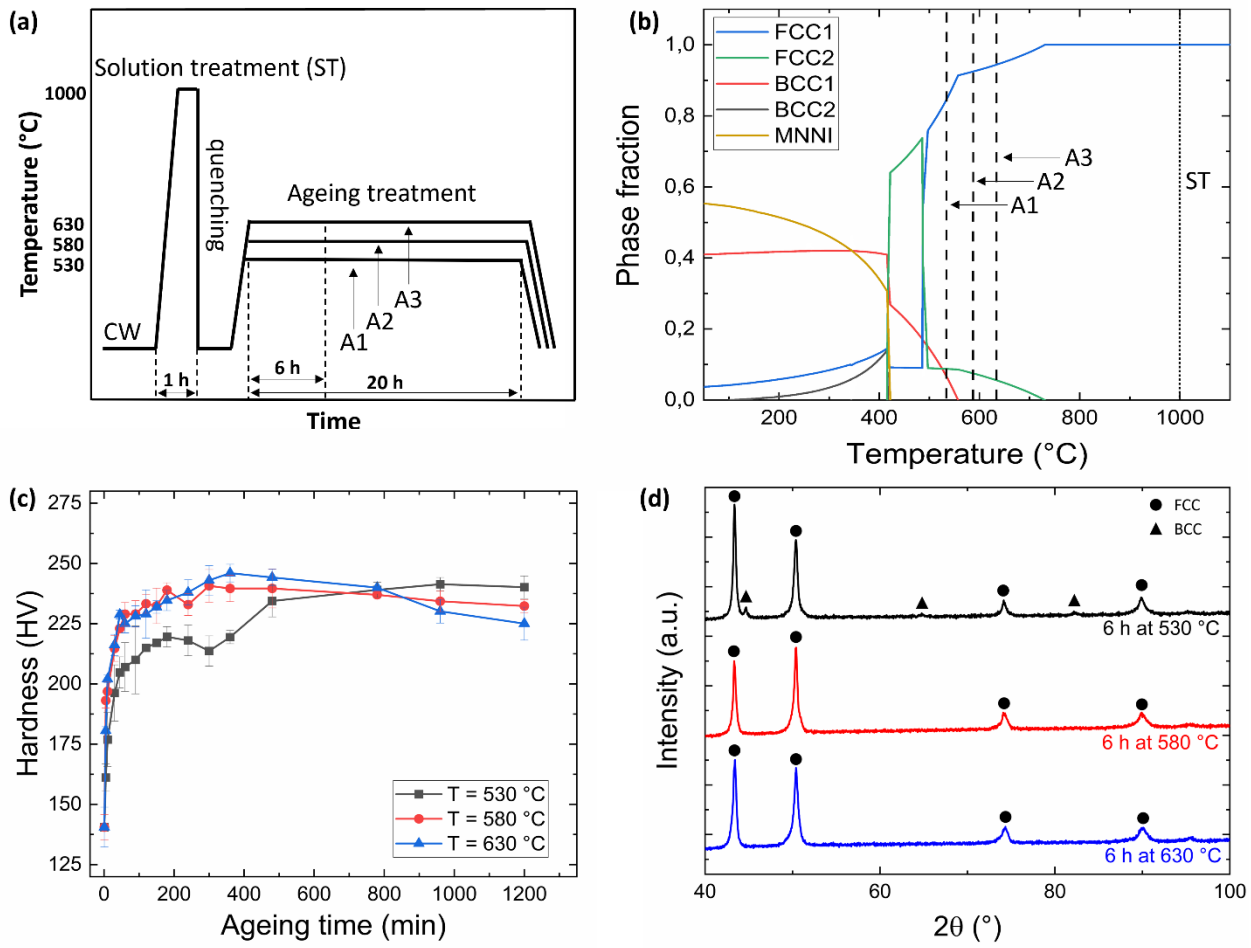


Figure 1: (a) schematic depicting the heat treatment schedules; (b) CALPHAD-computed equilibrium step-diagram of the CoCuFeMnNi alloy; (c) ageing curves collected at 530 °C, 580 °C and 630 °C; (d) XRD diffractogram obtained from samples aged for 6 h at different temperatures.

Figures 2, 3 and 4 show the results of FE-SEM, S-XRD and ac-STEM analyses on the CoCuFeMnNi alloy in the different heat-treatment conditions. The solution-treated alloy is composed of uniform grains, with an average size of about 20 µm, and, at a first glance, only faint rounded features are visible (Figure 2 a). However, the contrast variation observed in the annular dark-field (ADF) STEM images obtained from the grains in the solution-treated alloy (Figure 4 a) indicates that the rounded features observed in this alloy are induced by local compositional fluctuations. Such compositional fluctuations appear as coherent spherical-like shapes with diameter of about 5 to 10 nm. These spherical-like clusters show a brighter contrast compared to the matrix in the ADF image, implying that their density is higher than the matrix density. The EDX line scans (e.g. Figure 4 c) obtained across the features with bright contrast in ADF images indicate that those features have a higher Cu concentration compared to the matrix, which in turn results to be depleted in Cu. It shall be noted that these values can be to some extent affected by underlying

material and the clusters that appear in the image can lie at different depths. Similar features with comparable size and composition were also found with atom probe tomography in homogenized CoCuFeMnNi alloy [12,14,23]. In addition, a proper interface cannot be defined between these clusters and the matrix, as the boarders of such clusters are determined by compositional variations rather than by differences in crystal structure or a significant change in the lattice spacing. It is also worth noting that further round features (1-2 nm in size) showing slight variation in contrast (Figure 4 a, b) due to fluctuations in Fe and Co content (Figure 4 c) are also noticeable throughout the microstructure. Despite the presence of such chemical fluctuations, a single set of FCC peaks ($d_{(111)}$ = 3.616 Å) were observed by S-XRD (Figure 3 a), which is consistent with selected area electron diffraction patterns available in literature [12]. In this context, as shown below, the same technique makes possible to discern phases with slightly different cell parameter, even though they are not resolved on a laboratory instrument.

Ageing treatment at 630 °C was observed to induce a radical change in the microstructure: although it did not noticeably change the grain size, it caused the formation of several different second phases at both grain boundaries and cores (Figure 2 b). For instance, as shown in Figure 2, heat treatment altered the structure of the interior of grains into a maze-like structure along with round shaped particles. ADF-STEM and EDX results provided in Figure 4 revealed that such round features are discs of the same nature of the bright phase constituting maze structure. Thus, we can conclude that the structure of aged alloy is made up by discs that are orthogonally oriented along three directions. Similar microstructures were observed by Shim et al. [14] in the homogenized $CoCu_{1.7}FeMnNi$ alloy. Second phase particles with elongated shape are also found along grain boundaries (Figure 4 g, h). Interfaces between the matrix and both discs (Figure 6 e) and grain boundary phase (Figure 6 h) appear to be perfectly coherent. Discs and grain boundary second phases are both characterized by an evident Cu-enrichment (about 40 – 50 at.%) and Fe-, Co-depletion, but the latter are coarser. Cu-rich discs, approximately 60 nm in diameter and 15 nm thick, lie on all the $\{100\}_{FCC}$ crystallographic planes of the matrix. Moreover, Cu-poor areas (Cu content is about 10 at.%, Figure 6 i) are formed close to the Cu-rich grain boundary phase. In agreement with this microstructural description, the S-XRD diffractogram displays three sets of FCC peaks (Figure 3), whose corresponding lattice parameters appear to be mainly determined by the enrichment/depletion of large Cu atoms in each phase. Thus, the phases observed in the samples annealed at 630°C can be summarized as follow: the matrix (central peaks, $d_{(111)}$ = 3.612 Å, f = 44.6 %), the Cu-rich discs and Cu-rich grain boundary phase (low-angle peaks, $d_{(111)}$ = 3.626 Å, f = 26.8 %) and the Cu-poor areas (high-angle peak, $d_{(111)}$ = 3.600 Å, f = 28.6 %).

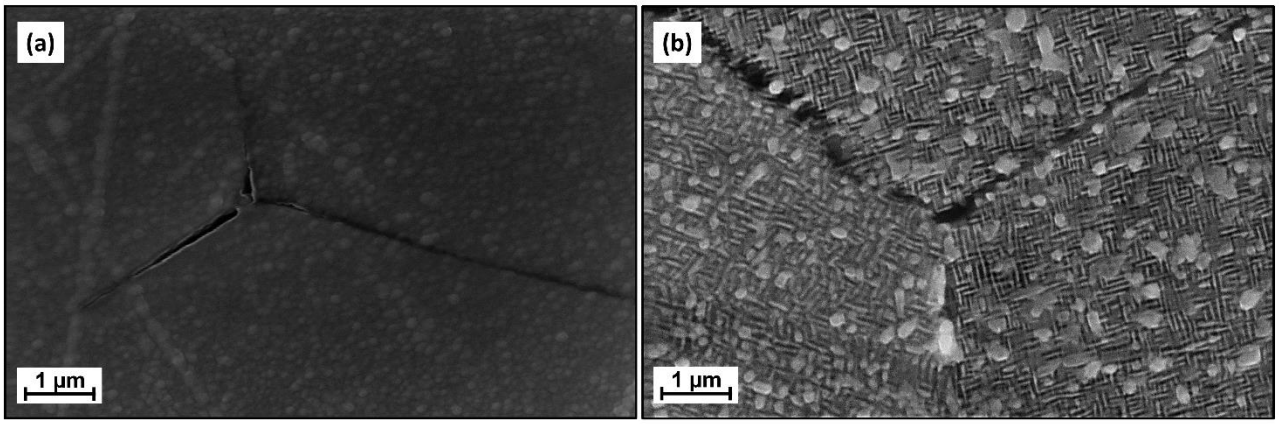


Figure 2: FE-SEM micrographs depicting the microstructure of CoCuFeMnNi alloy (a) in solution-treated and (b) peak-aged at 630 °C .

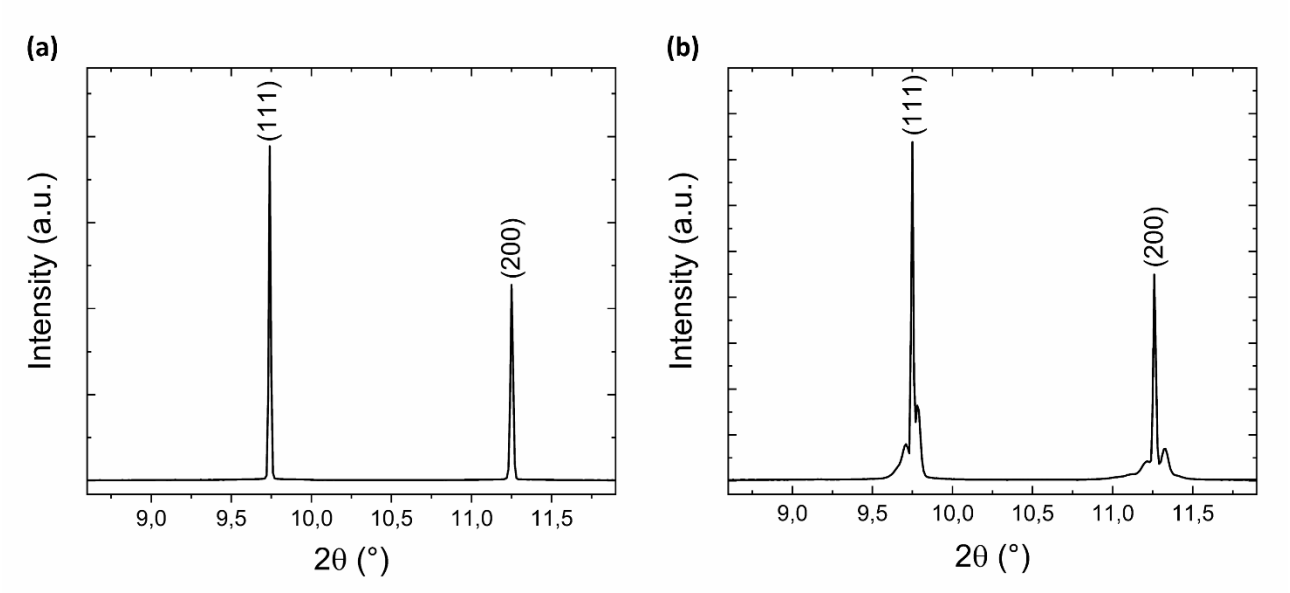


Figure 3: S-XRD patterns of CoCuFeMnNi alloy (a) in solution-treated condition and (b) peak-aged at 630 °C (magnified views of 8° to 12° showing (111) and (200) reflections).

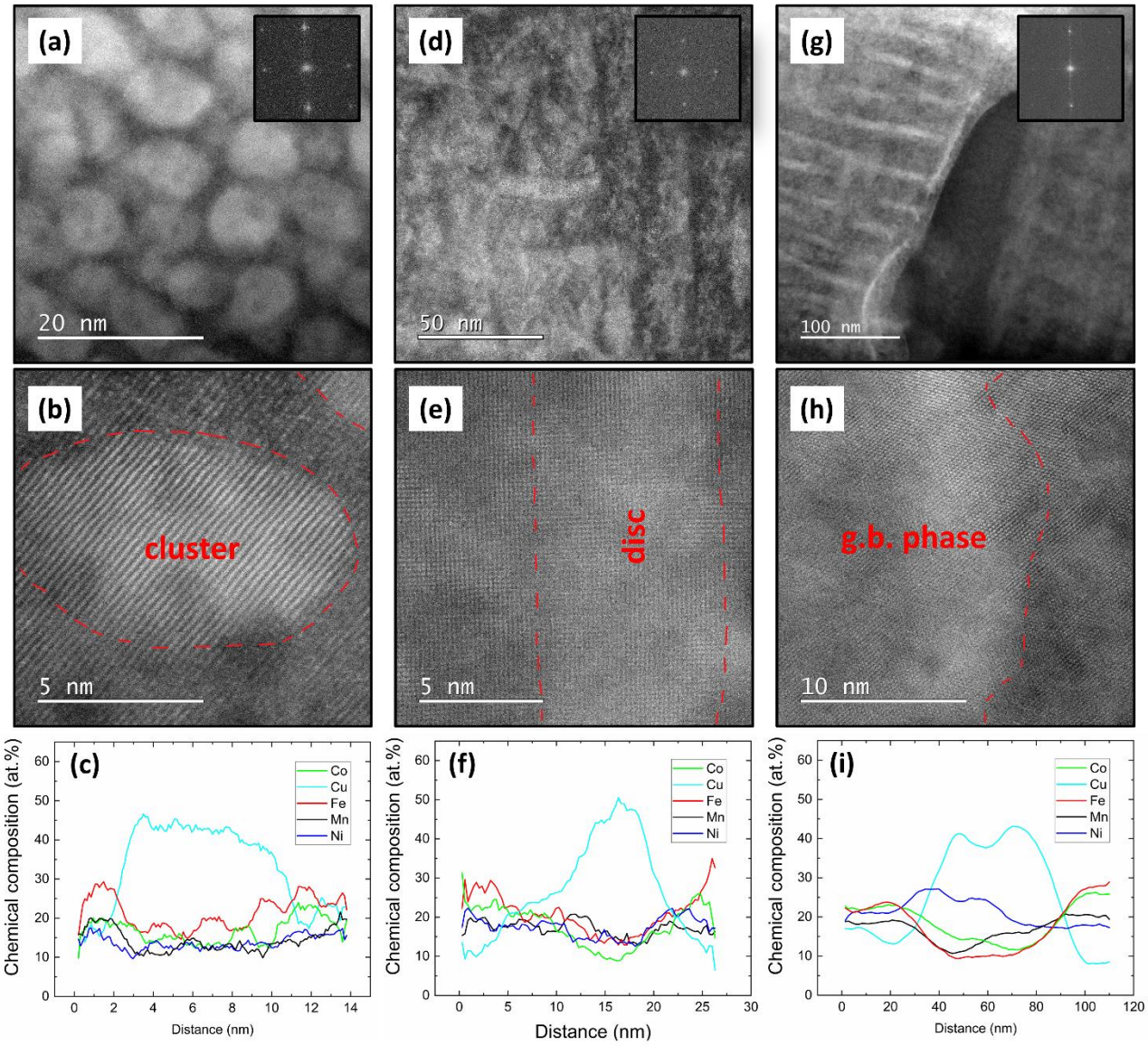


Figure 4: ADF-STEM images and EDS line scans obtained from the CoCuFeMnNi alloy in (a - c) solution-treated (d – i) and peak-aged at 630 °C conditions: (a, b, c) Cu-rich clusters in solution-treated condition; (d, e, f) Cu-rich rods in the maze-like structure; (g, h, i) grain-boundary phase in peak-aged condition. All ADF-STEM images show the $(100)_{FCC}$ crystallographic plane.

Similar geometric patterns were observed in other HEAs exhibiting both the FCC [24] and BCC [25,26] structures. Some works describe these phases as the result of a generic precipitation process [27,28]. Others refer to similar structures as the result of a spinodal decomposition, namely a phase separation process that does not include a nucleation step but derives from local compositional fluctuations leading to short-range diffusion and atomic clustering [29]. As a consequence, the two product phases usually show the same crystal structure and are only differentiated by chemical composition, with no distinct interface. Such characteristics could apply to the Cu-rich round clusters, which were found in solution-treated CoCuFeMnNi (Figure 4 a, b), and the mutually orthogonal Cu-rich discs detected in peak-aged samples

(Figure 4 d, e). Periodic compositional fluctuations, mainly consisting of Cu-enrichment and Fe-, Co-depletion, full structural coherency, and faint interfaces were indeed observed in such phases. Nevertheless, the presently available results cannot provide full confidence in discriminating between precipitation and spinodal transformations: further investigations, e.g. by means of atom probe tomography or small angle scattering (SAXS), could be useful to confirm the process leading to the formation of Cu-rich phases [30]. In particular, copper precipitation has been reported in several steels and HEAs [31], whereas spinodal decomposition through local compositional fluctuations and short-range diffusion was shown to take place even in concentrated FCC Fe - 50% Cu alloys obtained by mechanical alloying [32,33]. The decomposition of the supersaturated solid solution, taking place by spinodal decomposition or precipitation, is likely accompanied by stresses arising from the local variation of lattice parameter with composition [34], which likely favour the formation of the maze-like structure after ageing treatment [35].

As far as solution-treated samples are concerned, it shall be noted that CALPHAD simulation actually predicts the existence of a single FCC phase at 1000 °C. The existence of an evident phase separation is nevertheless evident and leads to the question whether such decomposition took place during holding at high temperature, upon quenching or, lastly, during ambient temperature storage as a sort of natural ageing. Previous works showed that spinodal decomposition can indeed take place in several materials, including both steels and HEAs, during rapid cooling from high temperature [36–38] and natural [39,40] and artificial [36,41] ageing. In both the solution-treated and peak-aged conditions, Cu atoms appear to be extremely prone to segregate from the disordered matrix. This tendency has been observed in other HEAs [31,42,43] and it is related to the large and positive mixing enthalpy, characterizing the interaction between Cu and other alloying elements (6 KJ/mol vs. Co, 13 KJ/mol vs. Fe, 4 KJ/mol vs. Mn and Ni [44]). It has also been reported that Cu segregation allows to minimize lattice strain energy in the considered alloy [14]. Therefore, it can be concluded that all the Cu-rich phases detected in peak-aged samples are actually the same phase originating from the unstable solid solution because of Cu tendency to segregate, and coincide with the Cu-rich FCC2 phase predicted by CALPHAD simulation and with the γ phase described in [12]. It shall be noted that ageing treatments at 530 °C and 580 °C would likely result in similar phase compositions, apart from the formation of a BCC phase after annealing at 530 °C. Indeed, as CALPHAD simulation predicts the stability of the Cu-rich FCC2 phase at both 530 °C and 580 °C, it is reasonable to expect that a decomposition of the supersaturated solid solution would result in a phase separation leading to the intercalation of Cu-rich and Cu-poor areas.

The effect of microstructural evolution on mechanical behaviour of the considered alloys was investigated through tensile tests at both ambient (25 °C) and cryogenic (-70 °C) temperatures. Representative stress – strain curves of the solution-treated and peak-aged alloy are depicted in Figure 5. At ambient temperature,

the ageing treatment causes an increase in the yield strength (YS) from 208 ± 4 MPa to 398 ± 7 MPa and ultimate tensile strength (UTS) from 516 ± 9 MPa to 642 ± 5 MPa. Conversely, fracture elongation ($\varepsilon_f$) was reduced from 28.3 ± 0.1 % to 18.5 ± 0.3 %. Differently from the typical behaviour of conventional alloys, lower temperature resulted in an improvement in both the strength (YS = 300 ± 10 MPa and UTS = 635 ± 15 MPa) and ductility ($\varepsilon_f$ = 31.2 ± 0,2 %) of the solution-treated alloy. Similarly, aged samples showed larger YS (449 ± 12 MPa), UTS (771 ± 17 MPa) and $\varepsilon_f$ (20.3 ± 0.3 %) at cryogenic temperature. These results show that the controlled ageing treatment can strongly improve the alloy's mechanical resistance, as yield strength shows an increase of almost 100 % with respect to the solution-treated condition. Indeed, it has been shown in previous works [45,46] that similar intercalated microstructures can positively affect material strength: the resulting lattice misfit generates a continuous modulation of local stress fields and elastic properties, which hinder the motion of dislocations [47].

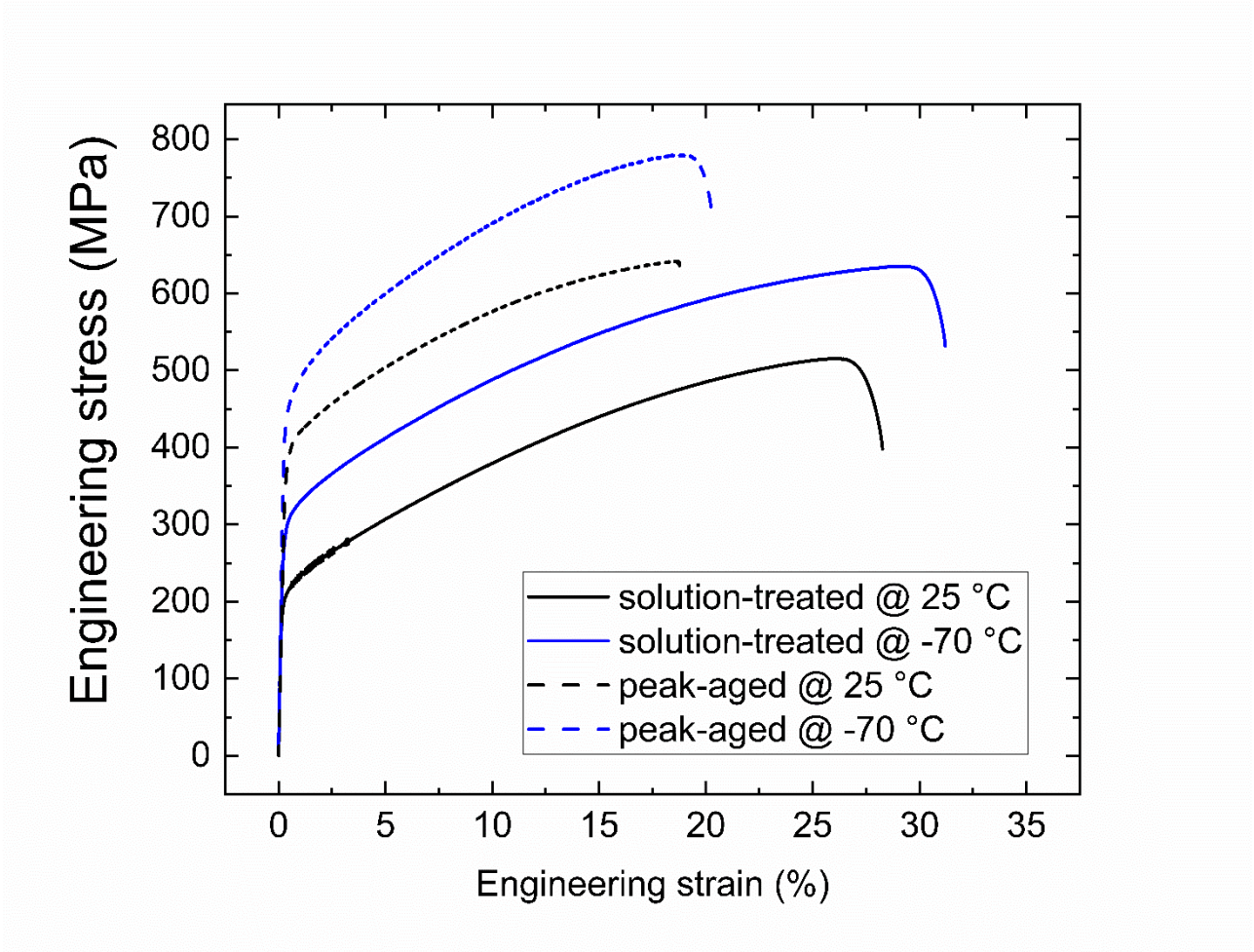


Figure 5: Representative engineering stress – strain curves at room temperature and -70 °C of the CoCuFeMnNi alloy in the solution-treated and peak-aged at 630 °C conditions.

It is of particular interest that both mechanical resistance and ductility are improved at cryogenic temperature. While the improvement in strength is related to the increase of critical resolved shear stress,

which is frequently observed at low temperature in most of structural alloys [48], the improved ductility may be related to the activation of different deformation mechanisms. In order to try and shed light on this aspect, the strain hardening parameter Θ was computed as $\Theta = \frac{\partial \sigma}{\partial \varepsilon}$, where σ and ε are true stress and true strain, respectively. The obtained curves of strain hardening as a function of the plastic strain and deformation temperature are depicted in Figure 6. Similar trends characterize all the studied conditions: after a fast decay during initial plastic deformation (Stage I) a softer decrease takes place until Considére's criterion (Θ = σ) is met, confirming that uniform elongation of the sample and localized necking take place before failure. The latter section is usually referred to as Stage III and is typical of alloys displaying a high stacking fault energy, such as aluminium or copper. Conversely, the intermediate presence of the so-called Stage II, characterized by a broad Θ peak, would indicate the activation of some peculiar deformation mechanism, including twinning and transformation induced plasticity [49]. In fact, it has been reported that twinning is frequently activated in FCC HEAs during deformation at low temperatures and allows to sustain elevated strain-hardening and accommodate large deformation [50]. Therefore, the absence of Stage II during the deformation of the present alloy may suggest that plasticity takes place by dislocation slip only, at both ambient and cryogenic temperatures. The present findings are in good agreement with those of Tazuddin et al. [10], who analysed the deformation behaviour of an homogenized CoCuFeMnNi alloy at room temperature and concluded that plasticity is mainly related to conventional octahedral slip. Similar conclusions were drawn by Shim and co-workers [14], who observed the formation of numerous grain-sized slip bands in deformed samples and suggested that Cu may raise the alloy's stacking fault energy with respect to other HEAs, such as the Cantor alloy. In full agreement with such results, we have observed deformation bands throughout solution-treated and peak-aged samples deformed at both ambient and cryogenic temperatures (Figure 7). Conversely, no deformation twin was found at this length scale.

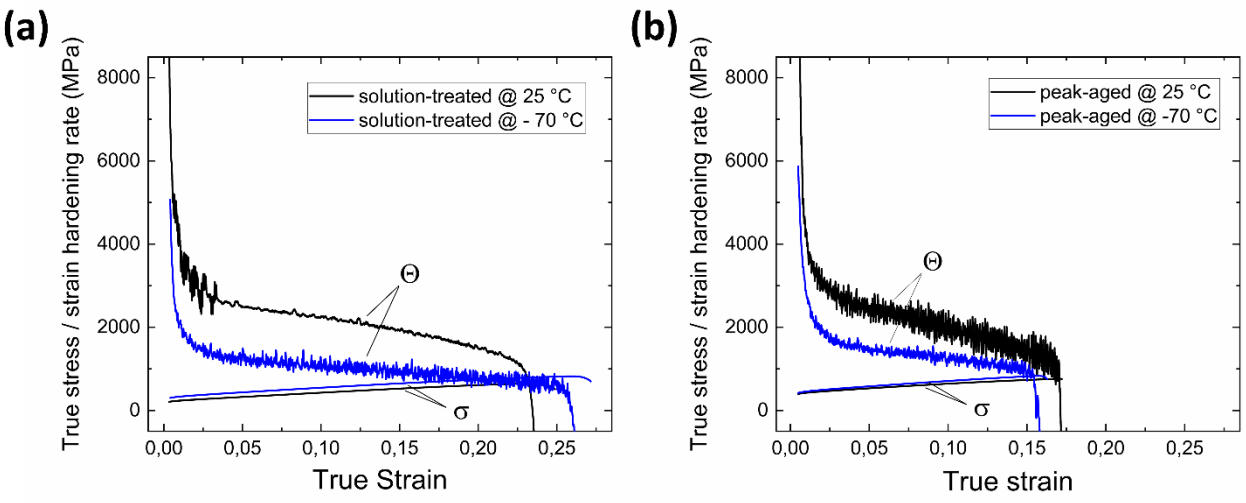


Figure 6: true stress-strain and strain hardening rate curves at room temperature and -70 °C of the CoCuFeMnNi alloy in the solution-treated and peak-aged at 630 °C conditions.

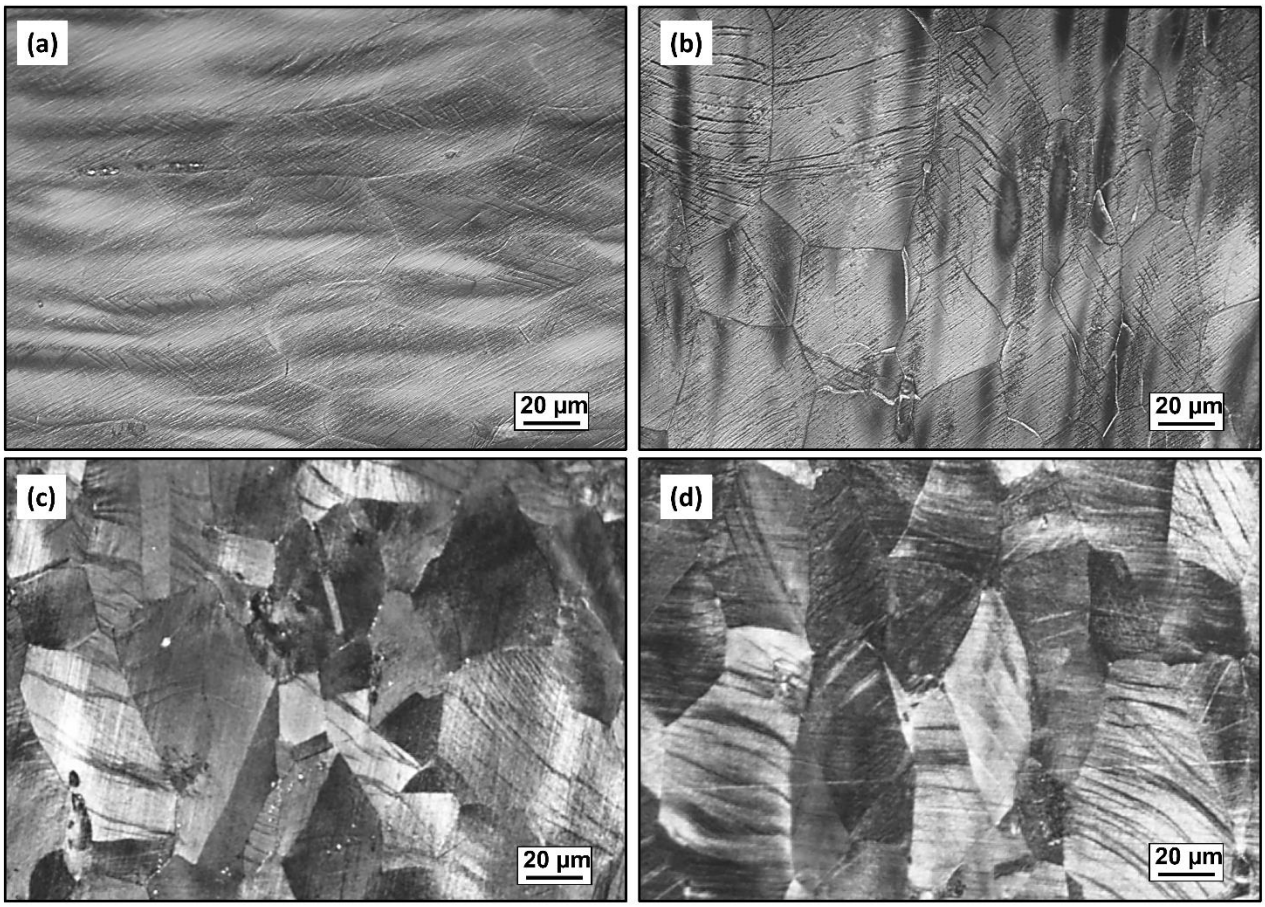


Figure 7: optical micrographs depicting deformation bands morphology in solution-treated (a, b) and peak-aged at 630 °C (c, d) samples tested at room temperature (a, c) and -70 °C (b, d).

## 4. Conclusions

To conclude, the present work shows that the inherent metastability of Cu-containing HEAs can be used to improve their mechanical behaviour through optimized thermal treatments, able to stimulate the formation of nanostructured and coherent second phases. Such phases create a continuous modulation of local composition and lattice parameters, which improve the alloy's strength. This is allowed by the presence of Cu, which shows higher atomic radius, lower shear modulus and a strong tendency to segregation. In particular, rounded Cu-rich clusters are detected in the solution-treated alloy. Conversely, regularly oriented, coherent, Cu-rich nanometric discs characterize the peak-aged condition and cause improved hardening of the alloy. Mechanical behaviour at low temperature is characterized by simultaneous enhancement of strength and ductility; plastic deformation appears to be based on dislocation slip, regardless of the testing temperature.

**Acknowledgements**

The authors would like to acknowledge Marco Pini, Nicola Bennato and Enrico Bassani from CNR ICMATE, Catherine Dejoie form ESRF, Paolo Pecoraro, Luca Signorelli, Lorenzo Giudici, Ludovica Rovatti and Rasheed Michael Ishola from Politecnico di Milano for their assistance in the experiments. Access to the David Cockayne Centre for Electron Microscopy (DCCEM) facilities of the University of Oxford was funded by the European Union's Horizon 2020 research and innovation programme under grant agreement No 823717 – ESTEEM3 (project ATHEnA). We acknowledge the ESRF for provision of beam time.

**References**

[1] E.P. George, D. Raabe, R.O. Ritchie, High-entropy alloys, Nat. Rev. Mater. 4 (2019) 515–534. doi:10.1038/s41578-019-0121-4.

[2] G. He, Y. Zhao, B. Gan, X. Sheng, Y. Liu, L. Tan, Mechanism of grain refinement in an equiatomic medium-entropy alloy CrCoNi during hot deformation, J. Alloys Compd. 815 (2020) 152382. doi:10.1016/j.jallcom.2019.152382.

[3] W. Wu, M. Song, S. Ni, J. Wang, Y. Liu, B. Liu, X. Liao, Dual mechanisms of grain refinement in a FeCoCrNi highentropy alloy processed by highpressure torsion, Sci. Rep. 7 (2017) 1–13. doi:10.1038/srep46720.

[4] D. Choudhuri, B. Gwalani, S. Gorsse, M. Komarasamy, S.A. Mantri, S.G. Srinivasan, R.S. Mishra, R. Banerjee, Enhancing strength and strain hardenability via deformation twinning in fcc-based high entropy alloys reinforced with intermetallic compounds, Acta Mater. 165 (2019) 420–430. doi:10.1016/j.actamat.2018.12.010.

[5] Z. Li, F. Körmann, B. Grabowski, J. Neugebauer, D. Raabe, Ab initio assisted design of quinary dual-phase high-entropy alloys with transformation-induced plasticity, Acta Mater. 136 (2017) 262–270. doi:10.1016/j.actamat.2017.07.023.

[6] S.S. Nene, M. Frank, K. Liu, R.S. Mishra, B.A. McWilliams, K.C. Cho, Extremely high strength and work hardening ability in a metastable high entropy alloy, Sci. Rep. 8 (2018) 1–8. doi:10.1038/s41598-018-28383-0.

[7] H. Diao, D. Ma, R. Feng, T. Liu, C. Pu, C. Zhang, W. Guo, J.D. Poplawsky, Y. Gao, P.K. Liaw, Novel NiAl-strengthened high entropy alloys with balanced tensile strength and ductility, Mater. Sci. Eng. A. 742 (2019) 636–647. doi:10.1016/j.msea.2018.11.055.

[8] B. Cantor, Multicomponent high-entropy Cantor alloys, Prog. Mater. Sci. (2020) 100754. doi:10.1016/j.pmatsci.2020.100754.

[9] Tazuddin, N.P. Gurao, K. Biswas, In the quest of single phase multi-component multiprincipal high entropy alloys, J. Alloys Compd. 697 (2017) 434–442. doi:10.1016/j.jallcom.2016.11.383.

[10] Tazuddin, K. Biswas, N.P. Gurao, Deciphering micro-mechanisms of plastic deformation in a novel single phase fcc-based MnFeCoNiCu high entropy alloy using crystallographic texture, Mater. Sci. Eng. A. 657 (2016) 224–233. doi:10.1016/j.msea.2016.01.065.

[11] R. Sonkusare, A. Swain, M.R. Rahul, S. Samal, N.P. Gurao, K. Biswas, S.S. Singh, N. Nayan, Establishing processing-microstructure-property paradigm in complex concentrated equiatomic CoCuFeMnNi alloy, Mater. Sci. Eng. A. 759 (2019) 415–429. doi:10.1016/j.msea.2019.04.096.

[12] R. Sonkusare, P. Divya Janani, N.P. Gurao, S. Sarkar, S. Sen, K.G. Pradeep, K. Biswas, Phase equilibria in equiatomic CoCuFeMnNi high entropy alloy, Mater. Chem. Phys. 210 (2018) 269–278.

doi:10.1016/j.matchemphys.2017.08.051.

[13] B.E. MacDonald, Z. Fu, X. Wang, Z. Li, W. Chen, Y. Zhou, D. Raabe, J. Schoenung, H. Hahn, E.J. Lavernia, Influence of phase decomposition on mechanical behavior of an equiatomic CoCuFeMnNi high entropy alloy, Acta Mater. 181 (2019) 25–35. doi:10.1016/j.actamat.2019.09.030.

[14] S.H. Shim, S.M. Oh, J. Lee, S.K. Hong, S.I. Hong, Nanoscale modulated structures by balanced distribution of atoms and mechanical/structural stabilities in CoCuFeMnNi high entropy alloys, Mater. Sci. Eng. A. 762 (2019) 138120. doi:10.1016/j.msea.2019.138120.

[15] I.J. Polmear, Light alloys: metallurgy of the light metals, John Wiley & Sons Australia, 1995.

[16] W. Sha, H. Leitner, Z. Guo, W. Xu, Phase transformations in maraging steels, Phase Transform. Steels. (2012) 332–362. doi:10.1533/9780857096111.2.332.

[17] A.K. Jena, M.C. Chaturvedi, The role of alloying elements in the design of nickel-base superalloys, J. Mater. Sci. 19 (1984) 3121–3139. doi:10.1007/BF00549796.

[18] Y. Yang, T. Chen, L. Tan, J.D. Poplawsky, K. An, Y. Wang, G.D. Samolyuk, K. Littrell, A.R. Lupini, A. Borisevich, E.P. George, Bifunctional nanoprecipitates strengthen and ductilize a medium-entropy alloy, Nature. 595 (2021) 245–249. doi:10.1038/s41586-021-03607-y.

[19] T. Yang, Y.L. Zhao, Y. Tong, Z.B. Jiao, J. Wei, J.X. Cai, X.D. Han, D. Chen, A. Hu, J.J. Kai, K. Lu, Y. Liu, C.T. Liu, Multicomponent intermetallic nanoparticles and superb mechanical behaviors of complex alloys, Science (80-. ). 362 (2018) 933–937. doi:10.1126/science.aas8815.

[20] H. Nam, C. Park, J. Moon, Y. Na, H. Kim, N. Kang, Laser weldability of cast and rolled high-entropy alloys for cryogenic applications, Mater. Sci. Eng. A. 742 (2019) 224–230. doi:10.1016/j.msea.2018.11.009.

[21] Y. Tong, D. Chen, B. Han, J. Wang, R. Feng, T. Yang, C. Zhao, Y.L. Zhao, W. Guo, Y. Shimizu, C.T. Liu, P.K. Liaw, K. Inoue, Y. Nagai, A. Hu, J.J. Kai, Outstanding tensile properties of a precipitation-strengthened FeCoNiCrTi0.2 high-entropy alloy at room and cryogenic temperatures, Acta Mater. 165 (2019) 228–240. doi:10.1016/j.actamat.2018.11.049.

[22] C. Dejoie, M. Coduri, S. Petitdemange, C. Giacobbe, E. Covacci, O. Grimaldi, P.O. Autran, M.W. Mogodi, D.Š. Jung, A.N. Fitch, Combining a nine-crystal multi-analyser stage with a two-dimensional detector for high-resolution powder X-ray diffraction, J. Appl. Crystallogr. 51 (2018) 1721–1733. doi:10.1107/S1600576718014589.

[23] R. Agarwal, R. Sonkusare, S.R. Jha, N.P. Gurao, K. Biswas, N. Nayan, Understanding the deformation behavior of CoCuFeMnNi high entropy alloy by investigating mechanical properties of binary ternary and quaternary alloy subsets, Mater. Des. 157 (2018) 539–550. doi:10.1016/j.matdes.2018.07.046.

[24] C.W. Tsai, Y.L. Chen, M.H. Tsai, J.W. Yeh, T.T. Shun, S.K. Chen, Deformation and annealing behaviors of high-entropy alloy Al0.5CoCrCuFeNi, J. Alloys Compd. 486 (2009) 427–435. doi:10.1016/j.jallcom.2009.06.182.

[25] Y.J. Zhou, Y. Zhang, T.N. Kim, G.L. Chen, Microstructure characterizations and strengthening mechanism of multi-principal component AlCoCrFeNiTi0.5 solid solution alloy with excellent mechanical properties, Mater. Lett. 62 (2008) 2673–2676. doi:10.1016/j.matlet.2008.01.011.

[26] J. Liu, H. Liu, P. Chen, J. Hao, Microstructural characterization and corrosion behaviour of AlCoCrFeNiTi x high-entropy alloy coatings fabricated by laser cladding, Surf. Coatings Technol. 361 (2019) 63–74. doi:10.1016/j.surfcoat.2019.01.044.

[27] C.M. Lin, H.L. Tsai, Equilibrium phase of high-entropy FeCoNiCrCu0.5 alloy at elevated temperature,

J. Alloys Compd. 489 (2010) 30–35. doi:10.1016/j.jallcom.2009.09.041.

[28] Y. Yang, G.D. Samolyuk, T. Chen, J.D. Poplawsky, A.R. Lupini, L. Tan, L. Ken, Coupling computational thermodynamics with density-function-theory based calculations to design L12 precipitates in Fe-Ni based alloys, Mater. Des. 191 (2020) 108592. doi:10.1016/j.matdes.2020.108592.

[29] F. Campbell, Elements of Metallurgy and Engineering Alloys, ASM International, 2008.

[30] A.H. Shinohara, K. Sugiyama, Y. Waseda, Novel application of anomalous small-Angle X-ray scattering to characterize inhomogeneities in materials, High Temp. Mater. Process. 10 (1992) 159–176. doi:10.1515/HTMP.1992.10.3.159.

[31] Y. Zhang, Z. Chen, D. Cao, J. Zhang, P. Zhang, Q. Tao, X. Yang, Concurrence of spinodal decomposition and nano-phase precipitation in a multi-component AlCoCrCuFeNi high-entropy alloy, J. Mater. Res. Technol. 8 (2019) 726–736. doi:10.1016/j.jmrt.2018.04.020.

[32] M.A. Turchanin, P.G. Agraval, I. V. Nikolaenko, Thermodynamics of alloys and phase equilibria in the copper-iron system, J. Phase Equilibria. 24 (2003) 307–319. doi:10.1361/105497103770330280.

[33] J.Z. Jiang, C. Gente, R. Bormann, Mechanical alloying in the Fe-Cu system, Mater. Sci. Eng. A. 242 (1998) 268–277. doi:10.1016/s0921-5093(97)00522-4.

[34] J.W. Cahn, On spinodal decomposition, Acta Metall. 9 (1967).

[35] Y.S. Li, S.X. Li, T.Y. Zhang, Effect of dislocations on spinodal decomposition in Fe-Cr alloys, J. Nucl. Mater. 395 (2009) 120–130. doi:10.1016/j.jnucmat.2009.10.042.

[36] W.C. Cheng, C.Y. Cheng, C.W. Hsu, D.E. Laughlin, Phase transformation of the L12 phase to kappa-carbide after spinodal decomposition and ordering in an Fe-C-Mn-Al austenitic steel, Mater. Sci. Eng. A. 642 (2015) 128–135. doi:10.1016/j.msea.2015.06.096.

[37] C. Mapelli, S. Barella, A. Gruttadauria, D. Mombelli, M. Bizzozero, X. Veys, γ Decomposition in Fe–Mn–Al–C lightweight steels, J. Mater. Res. Technol. 9 (2020) 4604–4616. doi:10.1016/j.jmrt.2020.02.088.

[38] A.M. Manzoni, H.M. Daoud, R. Voelkl, U. Glatzel, N. Wanderka, Influence of W, Mo and Ti trace elements on the phase separation in Al8Co17Cr17Cu8Fe17Ni33 based high entropy alloy, Ultramicroscopy. 159 (2015) 265–271. doi:10.1016/j.ultramic.2015.06.009.

[39] K.A. Taylor, L. Chang, G.B. Olson, G.D.W. Smith, M. Cohen, J.B.V. Sande, Spinodal decomposition during aging of Fe-Ni-C martensites, Metall. Trans. A. 20 (1989) 2717–2737. doi:10.1007/BF02670166.

[40] J.C. Zhao, M.R. Notis, Ordering transformation and spinodal decomposition in Au-Ni alloys, Metall. Mater. Trans. A Phys. Metall. Mater. Sci. 30 (1999) 707–716. doi:10.1007/s11661-999-0062-4.

[41] S. Wei, F. He, C.C. Tasan, Metastability in high-entropy alloys: A review, J. Mater. Res. 33 (2018) 2924–2937. doi:10.1557/jmr.2018.306.

[42] M.H. Tsai, H. Yuan, G. Cheng, W. Xu, K.Y. Tsai, C.W. Tsai, W.W. Jian, C.C. Juan, W.J. Shen, M.H. Chuang, J.W. Yeh, Y.T. Zhu, Morphology, structure and composition of precipitates in Al 0.3CoCrCu 0.5FeNi high-entropy alloy, Intermetallics. 32 (2013) 329–336. doi:10.1016/j.intermet.2012.07.036.

[43] C.J. Tong, Y.L. Chen, S.K. Chen, J.W. Yeh, T.T. Shun, C.H. Tsau, S.J. Lin, S.Y. Chang, Microstructure characterization of AlxCoCrCuFeNi high-entropy alloy system with multiprincipal elements, Metall. Mater. Trans. A Phys. Metall. Mater. Sci. 36 (2005) 881–893. doi:10.1007/s11661-005-0283-0.

[44] A. Takeuchi, A. Inoue, Classification of Bulk Metallic Glasses by Atomic Size Difference, Heat of Mixing and Period of Constituent Elements and Its Application to Characterization of the Main Alloying Element, Mater. Trans. 46 (2005) 2817–2829.

[45] M. Kato, T. Mori, L.H. Schwartz, Hardening by spinodal Modulated structure, Acta Metall. 28 (1980) 285–290.

[46] K. Sato, K. Tagawa, Y. Inoue, Spinodal decomposition and mechanical properties of an austenitic Fe-30wt.%Mn-9wt.%Al-0.9wt.%C alloy, Mater. Sci. Eng. A. 111 (1989) 45–50. doi:10.1016/0921-5093(89)90196-2.

[47] F. Léonard, R.C. Desai, Spinodal decomposition and dislocation lines in thin films and bulk materials, Phys. Rev. B - Condens. Matter Mater. Phys. 58 (1998) 8277–8288. doi:10.1103/PhysRevB.58.8277.

[48] W. Abuzaid, L. Patriarca, A study on slip activation for a coarse-grained and single crystalline CoCrNi medium entropy alloy, Intermetallics. 117 (2020) 106682. doi:10.1016/j.intermet.2019.106682.

[49] O. Bouaziz, S. Allain, C.P. Scott, P. Cugy, D. Barbier, High manganese austenitic twinning induced plasticity steels: A review of the microstructure properties relationships, Curr. Opin. Solid State Mater. Sci. 15 (2011) 141–168. doi:10.1016/j.cossms.2011.04.002.

[50] B. Gludovatz, A. Hohenwarter, D. Catoor, E.H. Chang, E.P. George, R.O. Ritchie, A fracture-resistant high-entropy alloy for cryogenic applications, 345 (2014) 1153–1159.